Dalton Transactions

Discriminatory behavior of a rhodamine 6G decorated mesoporous silica based multiple cation sensor towards Cu2+ and Hg2+ vis-à-vis Al3+, Cr3+ and Fe3+: Selective removal of Cu2+ and Hg2+ from aqueous medium

Journal:	*Dalton Transactions*
Manuscript ID	DT-ART-05-2021-001542.R2
Article Type:	Paper
Date Submitted by the Author:	18-Jun-2021
Complete List of Authors:	Singha, Debdas; Visva-Bharati, Integrated Science Education and Research Centre Pal, Ananya; Visva-Bharati, Integrated Science Education and Research Centre Uyama, Hiroshi; Osaka Univerisity, Roy, Partha; Jadavpur University Department of Chemistry, Nandi, Mahasweta ; Visva-Bharati, Integrated Science Education and Research Centre

Discriminatory behavior of a rhodamine 6G decorated mesoporous silica based multiple cation sensor towards Cu^{2+} and Hg^{2+} *vis-à-vis* Al^{3+}, Cr^{3+} and Fe^{3+}: Selective removal of Cu^{2+} and Hg^{2+} from aqueous medium

Debdas Singha,[a] Ananya Pal,[a] Hiroshi Uyama,[b] Partha Roy,[c] Mahasweta Nandi*,[a]

[a]*Integrated Science Education and Research Centre, Siksha Bhavana, Visva-Bharati University, Santiniketan 731 235, India*

Email: mahasweta.nandi@visva-bharati.ac.in (MN)

[b]*Department of Applied Chemistry, Graduate School of Engineering, Osaka University, 2-1 Yamadaoka, Suita, Osaka, 565-0871, Japan*

[c]*Department of Chemistry, Jadavpur University, Kolkata 700032, India*

Abstract

Selective identification of metal ions as well as their removal is possible when a sensing unit is anchored to a solid support. In this paper, functionalized mesoporous silica with pendant rhodamine 6G moiety (**R6FMS**) has been obtained by successive grafting of an aldehyde derivative of bisphenol A followed by rhodamine 6G over a 3-aminopropyl anchored mesoporous silica framework. The materials have been characterized by powder X-ray diffraction, nitrogen sorption and electron microscopic studies, FT-IR and solid state MAS NMR spectral studies, and thermal analysis. In ethanol, the colorless silica material gives pink coloration in the presence of Al^{3+}, Cr^{3+}, Fe^{3+} and Cu^{2+} which is also clearly evident from the generation of absorption peak at 525 nm. With excitation at 500 nm, fluorescence intensity of the probe increases by 36-, 17-, 40- and 89-fold in the presence of Al^{3+}, Cr^{3+}, Fe^{3+} and Cu^{2+} ions, respectively. This suggests **R6FMS** is a colorimetric and fluorescent chemosensor for these cations in ethanol. However, when solvent is changed from ethanol to water, it becomes a selective chemosensor only for Cu^{2+} and Hg^{2+}, by generation of pink color and strong fluorescence at *ca.* 550 nm thereby discriminating the trivalent cations. Cations induce opening of spirolactam ring resulting in pink coloration and strong fluorescence. Quantum yield and life time of the probe have been increased considerably in the presence of these cations in ethanol as well as aqueous media. Detection limit values for these cations lies in the range of 10^{-6} to10^{-8} M. **R6FMS** has been used to remove Hg^{2+} and Cu^{2+} from their aqueous solution with maximum adsorption capacity of 35 mg/g and 148 mg/g for Cu^{2+} and Hg^{2+}, respectively.

Keywords: Mesoporous silica; Rhodamine; Chemosensor; Multiple ions; Solvent dependent; Separation.

Introduction

Detection of cations by using fluorescent sensing is drawing special attention of the researchers over last few decades as use of the fluorescence technique offers advantages like high selectivity and sensitivity, low cost, simple procedure, non-destructive analysis, *etc*. There are considerable number of reports of fluorescent chemosensors which have been used for the detection of a single analyte.[1-3] In contrast, there are rather few examples of dual or multiple sensors[4,5] The most significant advantage of a dual or multiple ion sensor is that it can detect more than one species, and the process saves time and labor to generate chemosensors for each of the analytes individually. However, the major drawback of this type of chemosensor is that they could not discriminate all the analytes if interaction between the probe and analyte produces same output signal.[6-10] So, to develop an effective chemosensor for more than one species, it should be designed in such way that the probe interacts with various analytes in different ways. Other than that, variation in solvent can also play an important role to help to detect two species without much interference.[11-12] Even variation in solvent ratio, in some cases, may have controlling effect on the discriminatory behavior of a material.[13] On the other hand, by controlling pH of the medium it may be possible to tune the metal ion sensing properties of the probe.[14]

There are reports on rhodamine based probes for the detection of Al^{3+}, Cr^{3+} and Fe^{3+} ions as these cations induce increment in fluorescence as well as in absorption intensity.[15-17] On the other hand, Cu^{2+} or Hg^{2+} ions are also able to cause change in fluorescence and absorption properties of rhodamine derivatives.[18-20] Cr^{3+}, Fe^{3+} and Cu^{2+} are biologically relevant metal ions[21] and their deficiency or excess accumulation may have adverse effect on human health. Aluminum is present as the most abundant metal on the surface of the earth and its excessive deposition in our body has been related, in many research articles, to nerve related diseases such as Alzheimer's disease, Parkinson's disease, *etc*.[22,23] However, role of aluminum in this context is quite a debatable topic over many decades.[24] Many groups argued that there is no direct role of aluminum in Alzheimer's disease.[25] Mercury is undoubtedly toxic and its presence even in trace quantities is dangerous for the living world. It is produced by several anthropogenic activities which include mining operations, coal combustion, waste incineration, battery production, *etc*. along with volcanic eruption. It is commonly available in the Hg^0, Hg^+ and Hg^{2+} chemical states. Inorganic mercury, Hg^{2+}, is one of the most predominant toxic agents which may lead to damage of the kidneys and lungs.[26] The contamination of methylmercury as witnessed in Minamata disaster can impair functioning of the brain.[27] Hg^{2+} ions are widely distributed in aqueous medium and thus the fish and water that is consumed and having large quantity of mercury may give rise to severe health problems. Thus, detection of all these cations is important both for chemical and environmental sciences.

The process of detection provides additional benefit if the probe can also help to remove the target analyte by binding it strongly. The sensors which are insoluble in common solvents can perform

this task effectively. Polymers with appropriate functionalization are reported to display multifunctional properties towards sensing and separation.[28] MOFs with suitable binding sites, inherent or generated after post modification, can identify and also remove analytes.[29-31] In this respect, functionalized mesoporous silica materials can also be a great choice. Their robust structures with suitably introduced binding sites can detect a metal ion, bind to it strongly and finally separate it from the medium. Mesoporous silica is a good candidate for consideration as a solid support for functionalization with sensing units as its pore volume and pore size can be easily tuned. Incorporation of organic sensor part by covalent grafting not only provide sensing unit for the identification of the target analyte but also after its binding, the target species can be thrown out by simple filtration as the silica material is usually insoluble in common solvents. We have developed 2-hydroxy-1-naphthaldehyde functionalized material to sense Al^{3+} and remove it from solution[32] and incorporated a trialdehyde and 2-aminothiophenol onto a mesoporous silica material to detect and remove Hg^{2+} from aqueous solution.[33] Recently, we have reported rhodamine 6G incorporated mesoporous silica bound to terephthaldehyde to detect Al^{3+}, Cr^{3+} and Fe^{3+} and separate these cations.[34] In the present study, we wanted to replace the aldehyde with one that contains an extra donor atom and incorporate rhodamine 6G on the mesoporous silica framework in anticipation of observing its effect on metal ion sensing and removal properties.

With this background, we report here synthesis, characterization and metal ion sensing with a bisphenol A and rhodamine 6G incorporated mesoporous silica material (**R6FMS**) (Scheme 1). It is motivating to find that with the change in solvent media dramatic effect on the results have been observed. As fluorophoric moiety with donor centers has been anchored to silica framework, **R6FMS** could be utilised to both detect and remove metal ions from their aqueous solutions.

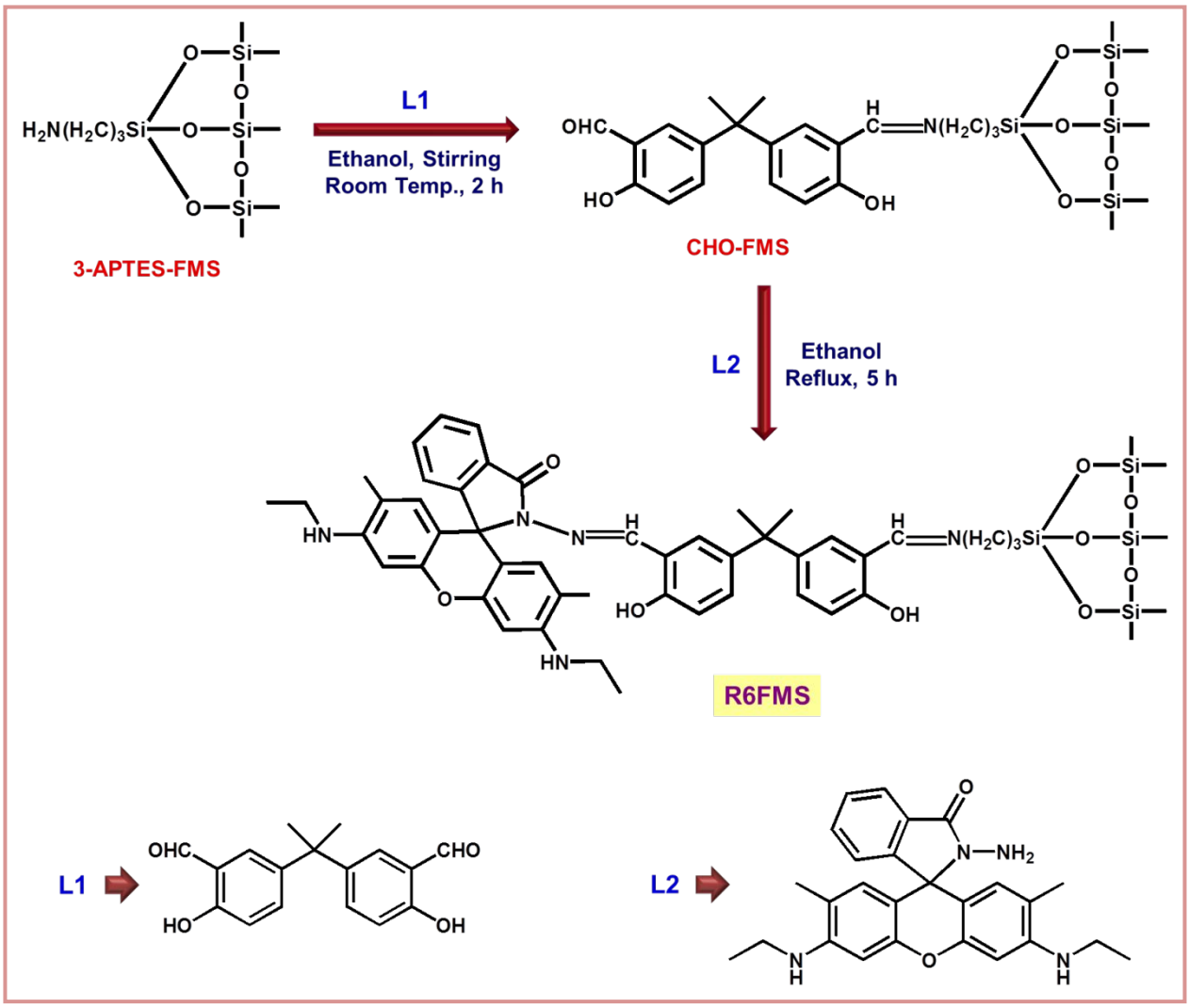

Scheme 1. Synthesis of **R6FMS**.

Experimental Section

Materials and Physical methods

Tetraethyl orthosilane (TEOS), cetyltrimethyl ammonium bromide (CTAB), rhodamine 6G, 3-aminopropyltriethoxysilane (3-APTES), bisphenol A, trifluoroacetic acid (TFA), various metal salts and other chemicals were purchased from commercial sources and used without further purification. Solvents used for the spectroscopic studies have been purified and dried following standard methods[35] prior to use. The X-ray powder diffraction patterns of the samples have been obtained using a Bruker D-8 Advance instrument using Ni-filtered Cu-Kα radiation (λ =1.5406 Å) at 40 kV and 40 mA. Nitrogen adsorption/desorption isotherms of the samples at various stages of functionalization have been measured at 77 K using a NOVA 2200e pore size and surface area analyzer, Quantachrome Instruments, USA. The samples were degassed before measurements for 6 hours at 353 or 423 K according to the composition of the functionalized materials. The specific surface areas of the samples were determined using multipoint BET (Brunauer-Emmett-Teller) method whereas the pore size distribution plots were obtained by employing NLDFT (Non-local Density Functional Theory) model. Field emission-scanning electron microscopic (FE-SEM) images have been recorded using a Zeiss make Gemini SEM 450 microscope equipped with EDAX Ametek (Model: Element) energy dispersive spectroscopy (EDS) attachment. On the other hand, for recording the transmission electron microscopic (TEM) image a JEOL JEM-1400 transmission electron microscope was used. Sample grid has been prepared by casting a drop of the sample dispersed in ethyl alcohol on a thin layer of copper grid of 400 mesh coated with amorphous carbon. FT-IR spectra of the samples are obtained on a Shimadzu IRAffinity-1S Fourier transform infrared spectrometer (Spectrum Two) using KBr pellets. Solid state MAS NMR spectra of the samples have been carried out using a CHEMAGNETICS 300 MHz CMX 300 spectrometer. Thermogravimetric analyses (TGA) have been carried out using a TA SDT 650 instrument under nitrogen atmosphere (flow rate: 100 ml/min) in the temperature range of 303–1173 K at a heating rate of 10 K min^{-1}. Absorption spectra have been recorded on a Shimadzu UV-2450 spectrophotometer using cuvettes of path length (*l*) 1 cm and emission spectra were obtained using a Horiba make FluoroMax-4C spectrophotometer. Luminescence lifetime measurements were carried out using a time-correlated single photon counting set up from Horiba Jobin-Yvon. The luminescence decay data have been collected on a Hamamatsu MCP photomultiplier (R3809) and were analyzed using the IBH DAS6 software. Emission intensities of the probe in the presence of different metal ions were recorded using their chloride salts unless stated otherwise.

Synthesis

Synthesis of L1 and L2

L1 was synthesized following a procedure reported previously.[36] In a typical process, 0.50 g of bisphenol A (2.19 mmol) and 3.68 g of hexamethylenetetramine (HMTA, 26.25 mmol) were dissolved in trifluoroacetic acid (35 mL) and refluxed for 24 h (supplementary information, Scheme S1). Upon completion of the reaction, the mixture was cooled to room temperature followed by the addition of 100 mL 1.0 M HCl. The resulting mixture was extracted with 100 mL dichloromethane; the organic layer was washed with water thrice and with saturated brine once, and dried over $MgSO_4$. Removal of the solvent after filtration afforded the compound **L1** as a yellow oily product. The yield was found to be 75 %.

The rhodamine derivative, **L2**, was also synthesized following a published procedure.[37] For that, a solution of 1.50 g of rhodamine 6G and 2.50 mL of anhydrous hydrazine in 30 mL of ethanol was heated to reflux for 10 h under nitrogen atmosphere (Scheme S1). After cooling, the solution was poured into cold water. The crude product was filtered off and purified by washing repeatedly with a mixture of solvent containing ethanol/water (*v/v* = 4/6).

Synthesis of R6FMS

SBA-15 type of mesoporous silica (**MS**) has been used here to act as the solid support and it has been synthesized following a published procedure.[33] In a typical batch, 3.40 g of the block copolymer surfactant, Pluronic P123, was first dissolved in 125 mL of water taken in a polypropylene bottle by stirring. Then 12 g of 35% HCl solution was added to the resulting clear solution and stirred for another 30 min. Finally, 7.00 g of TEOS was added dropwise, the mixture was stirred for 24 h at 313 K and the resulting white gel was autoclaved and heated in an oven at 373 K for 20 h. Then the white mixture was cooled to ambient temperature and filtered followed by thorough washing with water and then ethanol. The white product was dried and calcined at 773 K for 10 h in a flow of air. The mesoporous silica that was obtained has been functionalized with 3-aminopropyl triethoxy silane (3-APTES) by stirring 2.50 g of the silica with 2.50 g of 3-APTES. The reaction is carried out in chloroform under nitrogen atmosphere and at room temperature for 10h. The 3-APTES functionalized mesoporous silica (**3-APTES-FMS**) was collected through filtration, washing several times with chloroform and then dichloromethane and finally drying in air.

R6FMS was synthesized from **3-APTES-FMS** in two steps (Scheme 1). At first, 2.00 g of **3-APTES-FMS**was allowed to react with 1.30 g of **L1** in ethanol in the presence of a drop of glacial acetic acid for 2 h at ambient temperature. The resulting pale-yellow solid (**CHO-FMS**) was separated by filtration, washed several times with ethanol and once with acetonitrile and dried in air. Next, 1.60 g of this product was dispersed in ethanol, mixed with 1.00 g of **L2** and refluxed under stirring again in the

presence of one drop of glacial acetic acid for 4 h. Filtering the suspension, washing the residue several times with ethanol followed by acetonitrile and drying in air gave the final yellow colored solid product, **R6FMS**.

Spectroscopic measurements

Absorption and fluorescence spectra of **R6FMS** were obtained in absence and in the presence of different metal cations by varying their concentrations in ethanol and also in water/acetonitrile (14:1, v/v) (pH 7.2, 10 mM HEPES buffer) at 298 K. Usually, chloride or nitrate salts of Al^{3+}, Cr^{3+}, Fe^{3+}, Na^{+}, K^{+}, Mg^{2+}, Ca^{2+}, Mn^{2+}, Co^{2+}, Ni^{2+}, Cu^{2+}, Zn^{2+}, Cd^{2+}, As^{3+}, Hg^{2+} and Pb^{2+} were used for the measurements (Table S1). The probe was taken either in ethanol or in water/acetonitrile (14:1, *v/v*) (pH 7.2, 10 mM HEPES buffer) and sonicated for 10 min before recording the spectral data. Typically, for all the spectroscopic measurements, the probe in the respective media and metal ion were mixed to get final concentration of the probe as 0.033 g/L with desired concentration of the cation.

Determination of quantum yield

Fluorescence quantum yields (Φ) of **R6FMS** and Al^{3+}, Cr^{3+}, Fe^{3+}, Cu^{2+} and Hg^{2+} bound **R6FMS** were determined using the following formula:

$$\Phi_{sample} = \{(OD_{standard} \times A_{sample} \times \eta^2_{sample})/(OD_{sample} \times A_{standard} \times \eta^2_{standard})\} \times \Phi_{standard}$$

where A is the area under fluorescence emission curve, OD is the optical density of the sample at 500 nm (excitation wavelength) and η is the refractive index of the corresponding solvent. The quantum yields of all of the samples were determined using rhodamine-6G (0.94) as the standard.[38]

Separation of metal ions

Cu^{2+} or Hg^{2+} ions were removed from aqueous solution using **R6FMS** as the sorbent following the same procedure. Cation removing efficiency of the silica material was determined using same method for both the metal ions. For this purpose, 10 mL of 50 ppm for Cu^{2+} and 10 mL of 88 ppm Hg^{2+} ion solution was treated separately with 0.025 g of **R6FMS** under stirring condition for half an hour. Metal bound **R6FMS** was then removed from the solution by filtration. The filtrate obtained was analyzed to determine the final metal ion concentration. For the determination of maximum adsorption capacity of the probe, 0.025 g of **R6FMS** was treated with 10 mL of 50 g per litre metal ion solution. Initial concentration of metal ion in the solution and concentration of metal ion in the filtrate after treatment with and separation from silica matrix were determined by AAS. The amount of metal in the cation bound probe was evaluated by digesting and extracting the solid Cu^{2+} or Hg^{2+} bound **R6FMS** using AAS.

Result and discussion

Synthesis of R6FMS

Synthesis of the probe, **R6FMS**, has been schematically depicted (Scheme 1). 3-APTES has been incorporated into mesoporous silica framework to get **3-APTES-FMS** following a published procedure.[33] Bisphenol A **(L1**) and rhodamine derivative (**L2**) have also been obtained following literature methods (Scheme S1).[36, 37] The Schiff-base condensation between **3-APTES-FMS** and **L1** has been carried out in such a way to obtain **CHO-FMS** where one of the aldehyde groups of **L1** remains unreacted. This condensation leads to covalent anchoring of bisphenol derivative into functionalized mesoporous silica with one pendant –CHO group. Another Schiff-base condensation has been performed between **CHO-FMS** and **L2** to generate final product, **R6FMS**. In both the condensation reactions, small quantity of glacial acetic acid has been added which acts as catalyst.

Mesoporosity and microstructure

The powder X-ray diffraction patterns of the samples are shown in Fig. 1. The mesoporous silica support of SBA-15 type (**MS**) with larger pore size is found to have a 2D-hexagonal ordered mesostructure which is quite evident from the three prominent diffraction peaks which correspond to the 100, 110 and 200 planes (Fig. 1a). The *d*-spacing calculated using Bragg's law from the 2θ value corresponding to the 100 plane of this silica support is found to be 8.74 nm (λ =0.15406 nm). The diffraction patterns for 3-APTES functionalized mesoporous silica (**3-APTES-FMS**), **L1** grafted silica (**CHO-FMS**) and the fluorophore (**L2**) attached final material (**R6FMS**) are also shown in Fig. 1 (b, c and d, respectively). The patterns indicate that after sequential functionalization of the **MS** with 3-APTES, **L1** and **L2** the ordered arrangement of pores is more or less retained but the intensities of the peaks diminish. In addition to that, the peak positions gradually shift to higher values of 2θ, indicating somewhat decrease in the *d*-spacing and is attributed to the shrinkage of pore diameters to some extent on each step of functionalization.

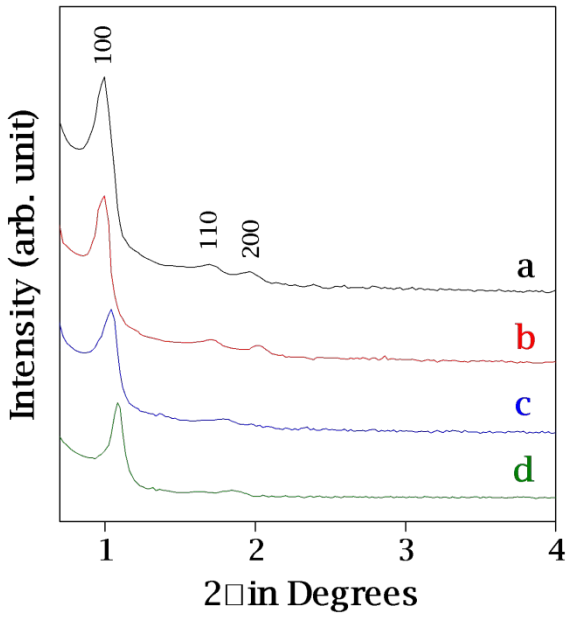

Fig. 1. Powder X-ray diffraction patterns of (a) mesoporous silica (**MS**), (b) **3-APTES-FMS**, (c) **CHO-FMS** and (d) **R6FMS**.

The nitrogen adsorption/desorption isotherms have been recorded for all the samples at various stages of functionalization. The isotherms for **MS**, **3-APTES-FMS**, **CHO-FMS** and **R6FMS** are given in Fig. 2. The corresponding NLDFT pore size distribution has been displayed in the inset. The BET surface areas, pore sizes and pore volumes of the samples are listed in Table 1. The silica support, **MS**, has a surface area of 720 m^2/g with the pore size distribution centered at 8.29 nm. Thus, the pore size obtained is well in agreement with that calculated from the X-ray diffraction pattern. On gradual functionalization, decrease in surface area as well as pore size and pore volume take place indicating that the mesopores of **MS** getting occupied with the functional groups. All the samples maintained a characteristic type IV isotherm typical of mesoporous structures[39] with steep rise due to capillary condensation at higher pressure. The broad H1-type hysteresis is attributed to the presence of 1D cylindrical channel[40] in the materials which can also be witnessed in the electron microscopic images of the final sample shown in the following section. The pore size of the final material, **R6FMS**, obtained after functionalization with **L1** followed by **L2** decreases considerably as compared to **MS**. This material which has been used as a fluorometric and colorimetric probe in the present study has a pore dimension of 5.59 nm.

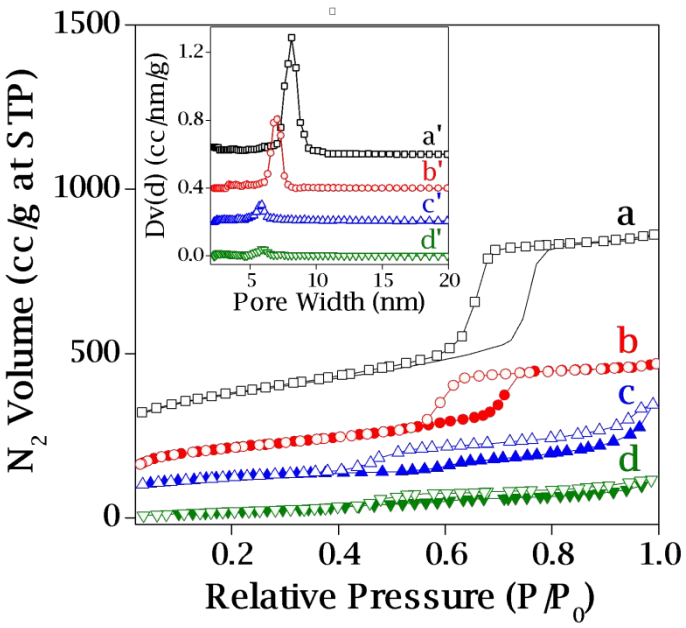

Fig. 2. Nitrogen adsorption/desorption isotherms of (a) mesoporous silica (**MS**), (b) **3-APTES-FMS**, (c) **CHO-FMS** and (d) **R6FMS**. For clarity, Y-axis values have been increased by 120, 120 and 60 cc/g for (a), (b) and (c), respectively. Filled symbols are for adsorption and empty symbols for desorption. **Inset:** Pore size distribution of (a') **MS**, (b') **3-APTES-FMS**, (c') **CHO-FMS** and (d') **R6FMS**. For clarity, Y axis values have been increased by 0.6, 0.4 and 0.2cc/nm/g for (a'), (b') and (c'), respectively.

Table 1. Surface area, pore volume and pore size distribution of different samples

Sl. no.	Sample	BET surface area (m^2/g)	Pore volume (cc/g)	Pore size (nm)
(a)	**MS**	720	1.068	8.29
(b)	**3-APTES-FMS**	326	0.500	7.05
(c)	**CHO-FMS**	196	0.438	5.83
(d)	**R6FMS**	109	0.177	5.59

The scanning and transmission electron microscopic images of **R6FMS** have been depicted in Fig. 3. As seen in the FE-SEM image (Fig. 3a), **R6FMS** obtained by functionalization of mesoporous SBA-15 type structure contains 1D cylindrical channel throughout the entire area of the sample under observation. In addition to that, the cross-section of the tubular channels of the mesoporous silica framework is also visible where the channels end. A closer picture is obtained from the TEM images (Fig. 3b). A selected area of a cylindrical channel has been magnified which shows the ordered arrangement of the pores and the morphology is in agreement with that obtained from FE-SEM studies. In the inset of

Fig. 3b, the TEM image of the cross section of the mouth of the tube is shown. It is evident from the image that the pores in **R6FMS** have an ordered hexagonal arrangement and the sizes of the pores are approximately 8 nm in diameter. This value is quite well in agreement with the *d*-spacing value calculated from X-ray diffraction studies. On the other hand, the pore width that is obtained from the NLDFT model of nitrogen sorption experiments gives somewhat lower value. This is the accessible pore size and the lowering is attributed to functionalization of the inner walls of the pore of the silica support with different organic moieties; it does not reflect the actual pore to pore distance of the mesoporous silica backbone.

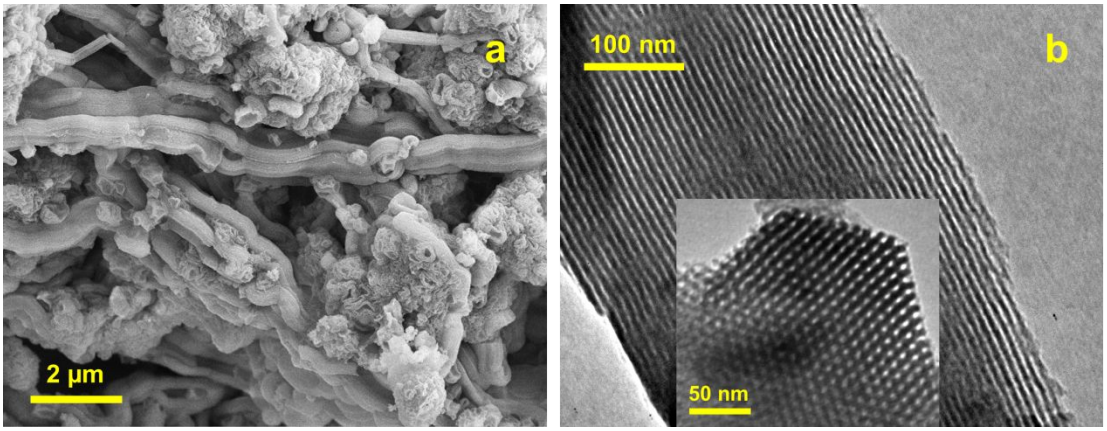

Fig. 3. (a) Field emission scanning electron microscopy (FE-SEM) image of **R6FMS** and (b) transmission electron microscopy image of **R6FMS**

FT-IR spectra and thermal studies

FT-IR spectra of **MS**, **3-APTES-FMS**, **CHO-FMS** and **R6FMS** are shown in supplementary information, Fig. S1. All the samples have shown strong band at 799 and 1055 cm^{-1}, which may be attributed to υ_s(Si–O) and υ_{as}(Si–O) bands, respectively. **CHO-FMS** (Fig. S1c) shows two bands at 1639 and 1703 cm^{-1} which indicate the presence of azomethine as well as unfunctionalized aldehyde group. Out of the two aldehyde groups one has been converted to imine moiety upon reaction with amine group of 3-APTES functionalized silica while the other aldehyde group remains free. Upon condensation with rhodamine moiety, **R6FMS** exhibits band at 1630-1635 cm^{-1} which indicates conversion of all the –CHO group to azomethine moiety (Fig. S1d, Table 2).

Thermogravimetric analyses have been carried out for all the samples to understand their thermal stabilities as well as to determine the amount of functionalization that has taken place on **MS** in each successive stage of functionalization. The results are shown in supplementary information, Fig. S2. It is clear from the figure that all of the silica materials show initial weight loss at the beginning at temperature around 350-400 K. This may happen due to loss of solvent, water. For mesoporous silica support (**MS**)

shown in Fig. S2a, it is evident that it is highly stable and the total amount of weight loss that takes place up to 1173 K is only *ca.* 11.06 %. This is mainly attributed to the presence of moisture in the sample and some other adsorbed species. Thermal analysis of the 3-APTES functionalized sample **3-APTES-FMS** (Fig. S2b) shows a total weight loss of *ca.* 23.11 % which takes place in two steps. The first loss from the beginning to around 393 K may be attributed to the presence of adsorbed water molecules in the sample, whereas the second one from 703 to 953 K is due to the burning of the aminopropyl unit. It has been calculated that 1.39 mmol/g of 3-APTES has been loaded into the silica framework. The plot for **L1** grafted sample **CHO-FMS** (Fig. S2c) shows similar behavior with weight loses at various steps corresponding to the functional groups and the total weight loss is *ca.* 31.3 %. Amount of bisphenol A incorporated has been found to be 0.29 mmol/g. Finally, for the rhodamine 6G derivative (**L2**) anchored material **R6FMS** (Fig. S2d), the weight loss takes place over the entire range corresponding to the removal of various organic components and the total weight loss is found to be *ca.* 33.98 % up to 1173 K. From here, the amount of **L2** incorporated into the framework has been ascertained to be 0.061 mmol/g.

Table 2. Peaks of FT-IR, ^{29}Si MAS NMR and ^{13}C CP MAS spectra of R6FMS and R6FMS after interaction after Al^{3+} and Hg^{2+}

Species	**Significant Peaks**
FT-IR spectra (cm^{-1})	
R6FMS	799, 1055, 1630-1635
^{29}Si MAS NMR spectra (ppm)	
R6FMS	–110.6, –102.3, –65.1, –58.2
R6FMS after interaction with Al^{3+} in ethanol	–109.8, –101.1, –66.7, –58.7
R6FMS after interaction with Hg^{2+} in ethanol	–110.5, –101.4, –66.9, –58.0
R6FMS after interaction with Hg^{2+} in aqueous buffer	–108.4, –101.5, –64.9, –58.6
^{13}C CP MAS spectra (ppm)	
CHO-FMS	10.5, 21.8, 29.9, 42.6, 117.2, 120.8, 126.9, 130.8, 132.8, 159.4, 166.4, 194.9

R6FMS	10.5, 15.1, 15.8, 16.2, 21.8, 24.5, 30.3, 36.2, 38.5, 41.2, 42.6, 66.3, 96.1, 98.1, 105.9, 117.5, 121.6, 123.0, 123.9, 126.7, 128.0, 128.6, 130.2, 133.7, 146.9, 151.4, 152.2, 154.1, 168.7
R6FMS after interaction with Al^{3+} in ethanol	9.8, 21.4, 43.3
R6FMS after interaction with Hg^{2+} in aqueous buffer	10.0, 15.0, 15.7, 22.3, 24.5, 25.1, 36.2, 38.4, 41.7, 42.7, 48.8, 95.7, 98.0, 106.0, 117.5, 121.6, 123.7, 126.6, 128.5, 130.4, 133.8, 147.0, 151.3, 152.3, 154.1, 157.0, 168.5

Solid state NMR studies

^{29}Si MAS NMR spectral analysis

^{29}Si MAS NMR spectra of mesoporous silica and its functionalized products at various stages have been obtained to know chemical environment of the silica center. ^{29}Si MAS NMR spectra of **MS**, **3-APTES-FMS**, **CHO-FMS** and **R6FMS** are given in supplementary information, Fig. S3. Mesoporous silica shows peaks at −110.6 and −102.3 ppm indicating the existence of Q^4 and Q^3 centers in the silica material. The peaks appear because of the presence $Si(OSi)_n(OH)_{4-n}$ species. However, when the silica framework has been successively functionalized with 3-APTES, **L1** and **L2**, the ^{29}Si MAS NMR spectra of **3-APTES-FMS**, **CHO-FMS** and **R6FMS** appear to be grossly similar (Fig. S3b-d). In addition to the peaks at −110.6 and −102.3 ppm, two new peaks emerge at around −65 and −58 ppm for **3-APTES-FMS**, **CHO-FMS** and **R6FMS** (Table 2). The peak around −65 ppm appears due to the T^3 ($(SiO)_3Si$-R-$Si(OSi)_3$) species whereas the peak at −58 ppm may be attributed to theT^2 ($(HO)_2(OSi)Si$-R-$Si(OSi)_2(OH)$)species, respectively.[32, 41]

^{13}C CP MAS spectral analysis

^{13}C CP MAS NMR spectra of compounds obtained during successive stages of synthesis have been recorded to check incorporation of corresponding organic moieties on silica frameworks. ^{13}C CP MAS NMR spectra of **3-APTES-FMS**, **CHO-FMS** and **R6FMS** have been shown in Fig. 4. Mesoporous silica after functionalization with 3-APTES shows peaks at 10.5, 22.2 and 42.8 ppm (Fig. 4a). These peaks may be attributed to the presence of three carbon atoms of propyl group. Peaks of ^{13}C CP MAS NMR spectrum of **CHO-FMS** are given in Table 2 which indicates incorporation of bisphenol A into the silica framework after Schiff-base condensation. Appearance of these peaks supports anchoring of

bisphenol A into **3-APTES-FMS**. Peaks at 10.5, 21.8 and 42.6 ppm confirm the retention of 3-APTES functionalized silica framework. Peak at 29.9 ppm may be attributed to methyl group of bisphenol A. However, peak at 166.4 ppm indicates conversion of one –CHO group into azomethine moiety. On the other hand, peak at 194.9 ppm indicates existence of one free aldehyde group in it. Peaks of carbon atoms of aromatic ring appear in their usual place. Peaks of **R6FMS** are given in Fig. 4c, Table 2. All of these peaks confirm incorporation of rhodamine unit *i.e.* **L2** into the **CHO-FMS** material. Peak at 194.9 ppm of **CHO-FMS** disappears in the spectrum of **R6FMS** indicating conversion of this aldehyde functionality into azothemine species.

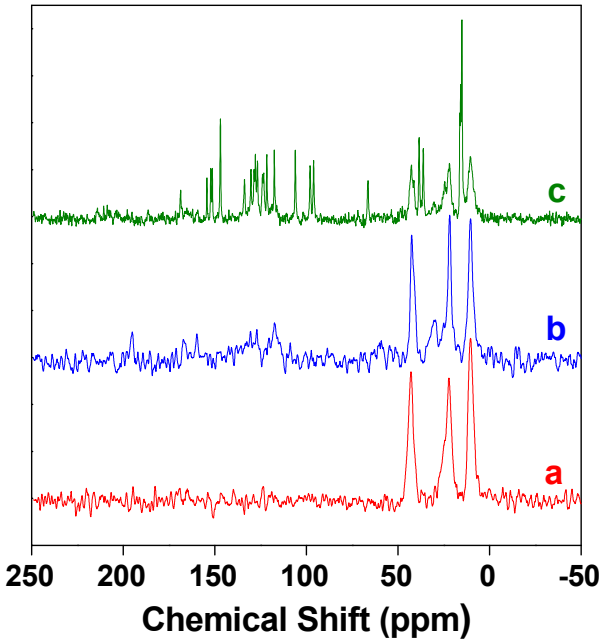

Fig. 4. Solid state ^{13}C CP-MAS NMR spectra of (a) **3-APTES-FMS**, (b) **CHO-FMS** and (c) **R6FMS**.

Absorption properties

Absorption spectra of **R6FMS** (0.033 g/L) are measured in absence and in the presence of different metal cations in two media. In ethanol, it does not show any observable band near 500 nm. However, there are several metal ions which induce significant change in the UV-vis spectrum of **R6FMS** in ethanol (supplementary information, Fig. S4). Among different metal ions, in the presence of trivalent cations such as Al^{3+}, Cr^{3+}, Fe^{3+} and a divalent cation, Cu^{2+}, it gives band at 525 nm with visual color change (Fig. 5). Absorbance of this band enhances gradually with increase in concentration (0 to 800 μM) of all of the trivalent cations (for Cu^{2+} it is 0 to 500 μM) as illustrated in Fig. 6 and Fig. S5. However, in addition to the 525 nm band, Cu^{2+} also produces a band at 630 nm with increasing intensity. Generation

of these bands indicates the opening of the spirocyclic ring of the probe and binding with the metal ion. **R6FMS** is colorless in absence of any cations as spirocyclic ring of the probe is in closed form. The cations induce the spirolactam ring opening leading to the generation of pink color as usual. However, other cations such as Na^{+}, K^{+}, Mg^{2+}, Ca^{2+}, Mn^{2+}, Co^{2+}, Ni^{2+}, Cu^{2+}, Zn^{2+}, Cd^{2+}, Hg^{2+} and Pb^{2+} fail to cause any color change as well as to create absorption band at around 500 nm (Fig. S4) indicating the fact that they are unable to open the spirolactam ring of **R6FMS** in ethanol.

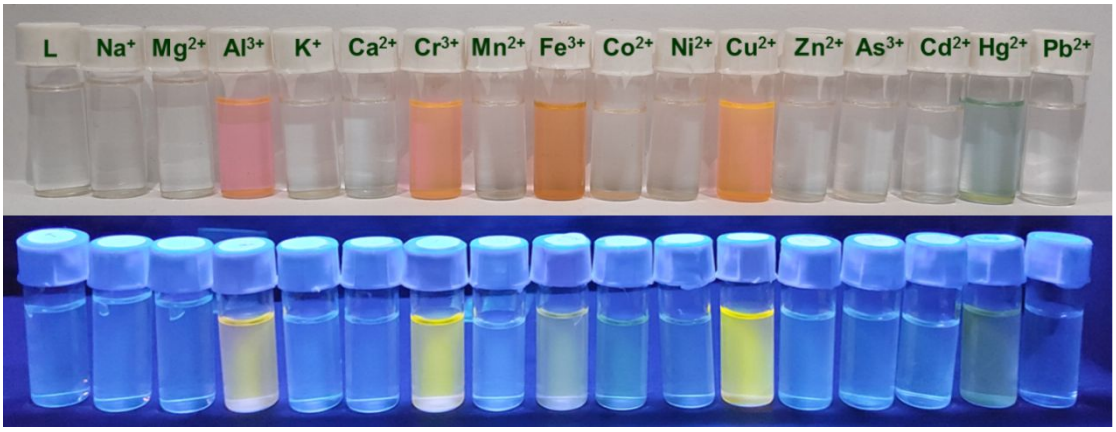

Fig. 5. Visual colorimetric change of **R6FMS** (**L**) in the presence of different metal ions under visible light (upper row) and UV light (lower row) in ethanol medium at 298 K.

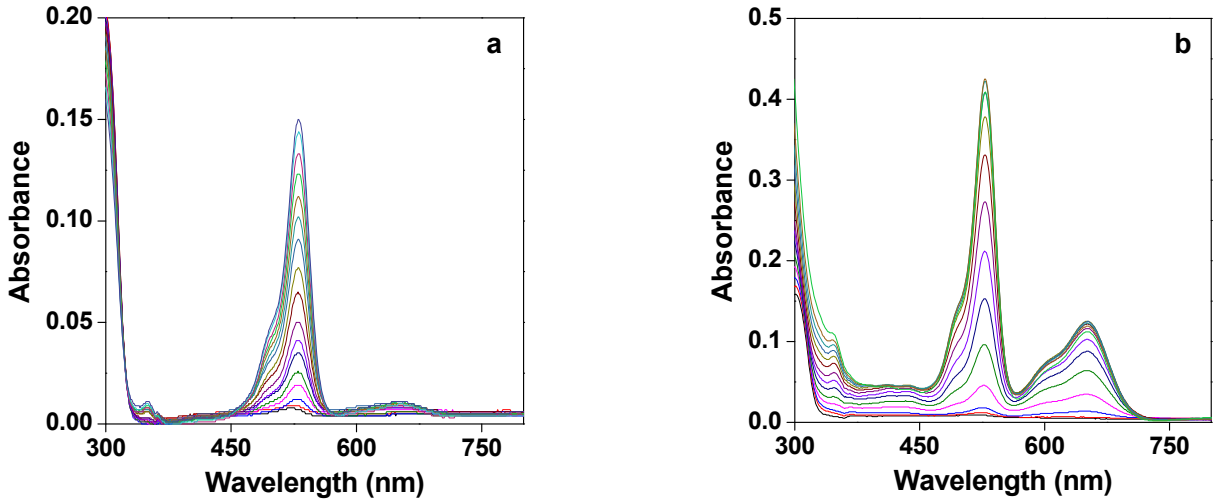

Fig. 6. Absorption spectra of **R6FMS** in the presence of different concentrations of (a) Al^{3+} (0-800 μM) and (b) Cu^{2+} (0-500 μM) in ethanol at 298 K (l = 1 cm).

There is sharp difference in the response of absorption spectral behaviour of **R6FMS** towards Al^{3+}, Cr^{3+}, Fe^{3+}, Cu^{2+} and Hg^{2+} if the solvent is changed from ethanol to water/acetonitrile (14:1, v/v) (pH 7.2, 10 mM HEPES buffer) (supplementary information, Fig. S6). There is no appearance of band at 525 nm in the UV-vis spectrum of the probe (0.033 g/L) in the presence of Al^{3+}, Cr^{3+} and Fe^{3+} in water/acetonitrile (14:1, v/v) (pH 7.2, 10 mM HEPES buffer). However, Cu^{2+} and Hg^{2+} give sharp changes in the spectral appearance of the probe with visual color change (Fig. 7). The pale yellow color for the Fe^{3+} ion solution comes from the ferric chloride salt that has been used for the study. However, it does not give any absorbance in the spectrum. Cu^{2+} and Hg^{2+} cations induce absorption bands at 525 nm and 625 nm with **R6FMS** in this medium like that in ethanol (Fig. 8). This means that these divalent cations can induce opening of spirocyclic ring of the probe with the generation pink coloration in aqueous buffer solution while the trivalent cations cannot open the spirolactam ring like they did in pure ethanol. Probably the trivalent cations are highly hydrated in buffer solution and cannot form coordination bond with the probe. All other monovalent, divalent cations also do not cause any visible change in the UV-vis spectrum of the probe in buffer medium. The possible speciation has been given in the supplementary information.

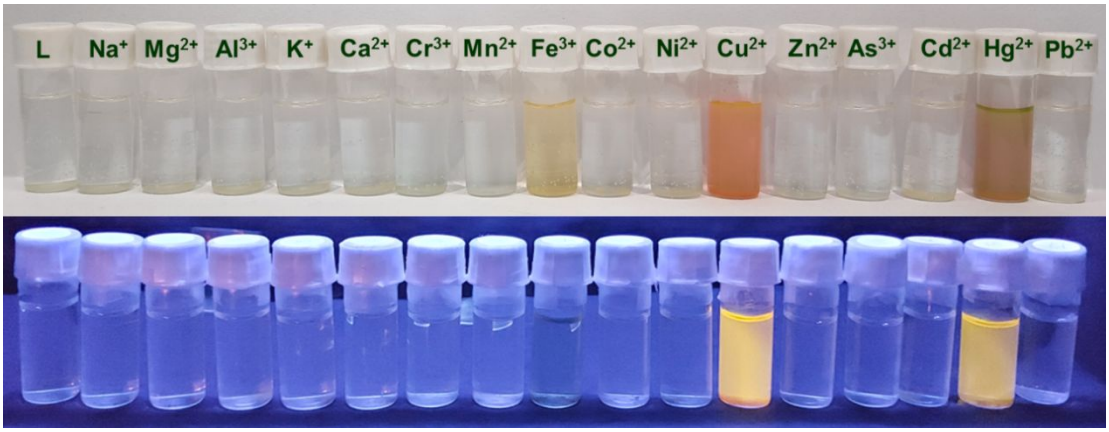

Fig. 7. Visual colorimetric change of **R6FMS** (**L**) in the presence of different metal ions under visible light (upper row) and UV light (lower row) in 10 mM HEPES buffer in water/acetonitrile = 14:1 (v/v) (pH 7.2) at 298 K.

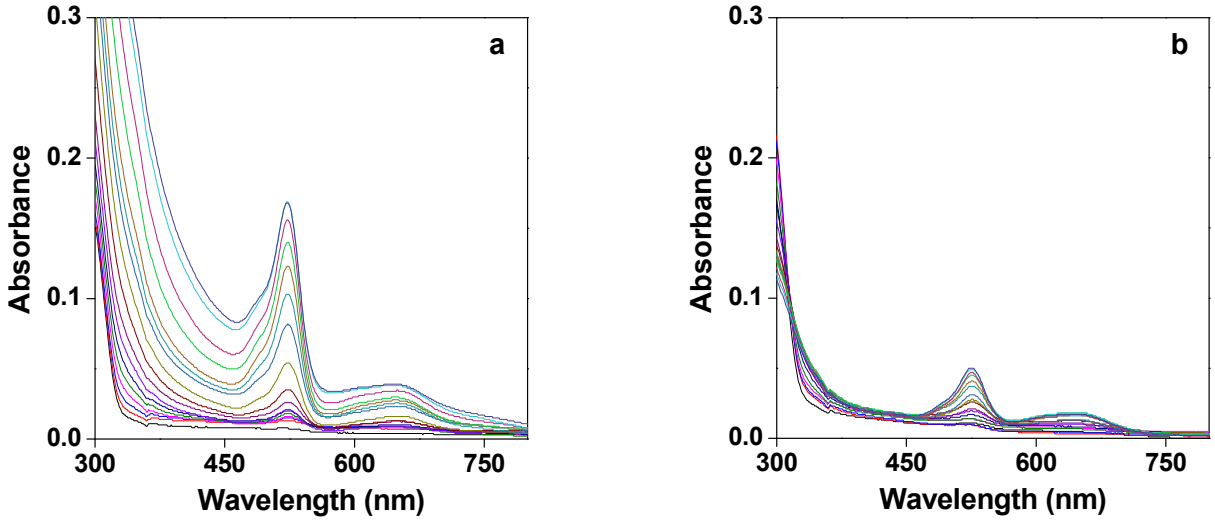

Fig. 8. Absorption spectra of **R6FMS** in the presence of (0-800 μM) (a) Cu^{2+} and (b) Hg^{2+} ions in 10 mM HEPES buffer in water/acetonitrile = 14:1 (v/v) (pH 7.2) at 298 K (l = 1 cm).

Fluorescence properties

As the probe behaved differently towards Al^{3+}, Cr^{3+}, Fe^{3+}, Cu^{2+} and Hg^{2+} ions in absorption spectroscopy in two different media, fluorescence spectra of **R6FMS** (0.033 g/L) have been recorded in absence and in the presence of different cations such as Al^{3+}, Cr^{3+}, Fe^{3+}, Na^{+}, K^{+}, Mg^{2+}, Ca^{2+}, Mn^{2+}, Co^{2+}, Ni^{2+}, Cu^{2+}, Zn^{2+}, Cd^{2+}, Hg^{2+} and Pb^{2+} in pure ethanol and also in water/acetonitrile (14:1, v/v) (pH 7.2, 10 mM HEPES buffer). The sensing behavior is anticipated to proceed *via* the interactions as shown in Scheme 2. When excited at 500 nm, **R6FMS** does not show any fluorescence in ethanol in absence of any metal cation (supplementary information, Fig. S7). But among the above mentioned metal ions, Al^{3+}, Cr^{3+}, Fe^{3+} and Cu^{2+} ions have been able to increase its fluorescence intensity at 550 nm. Fluorescence intensity increases with the gradual addition of these cations up to 800 μM (500 μM for Cu^{2+}) and then reaches saturation. Fluorescence intensity enhancement occurs by 36-, 17-, 40- and 89-fold in the presence of 800 μM of Al^{3+}, Cr^{3+}, Fe^{3+} and Cu^{2+} ions, respectively, in ethanol (Fig. 9 and Fig. S8). Generation of emission band at 550 nm indicates ring opening of the probe in the presence of these cations as also revealed in absorption spectral analysis, accompanied by pink coloration. Other relevant cations could not produce any significant fluorescence change of the probe. Effect of other metal ions on fluorescence intensity of **R6FMS** with Al^{3+} has been checked by recording fluorescence spectra of **R6FMS** with Al^{3+} (800 μM) in the presence of other cations (Fig. 10). It is clear from the figure that few of the cations including Ni^{2+}, Hg^{2+} and Pb^{2+} can decrease the fluorescence intensity of **R6FMS** with Al^{3+} mixture to some extent. This fact indicates that **R6FMS** can sense Al^{3+} ion in the presence of other cations in ethanol.

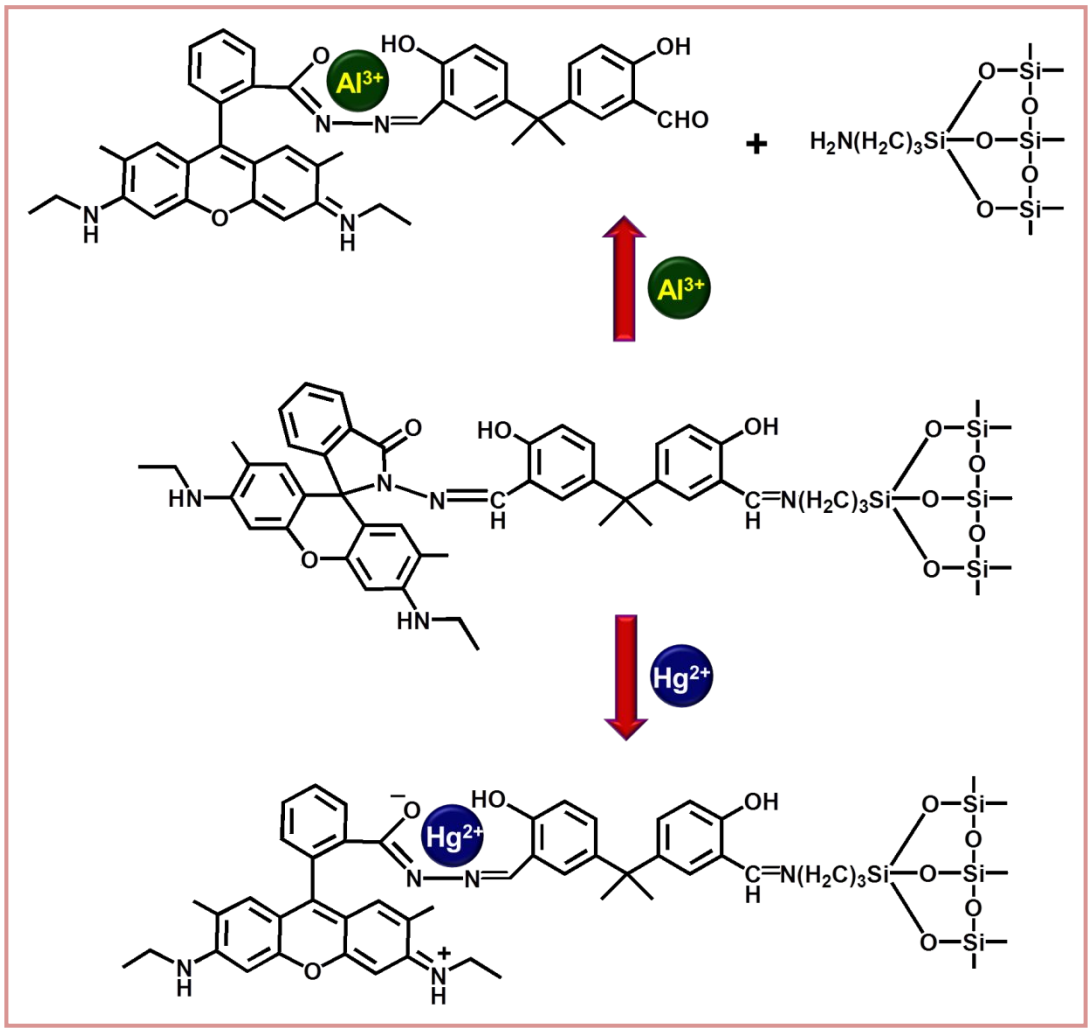

Scheme 2. Mechanism of metal ion sensing by **R6FMS**.

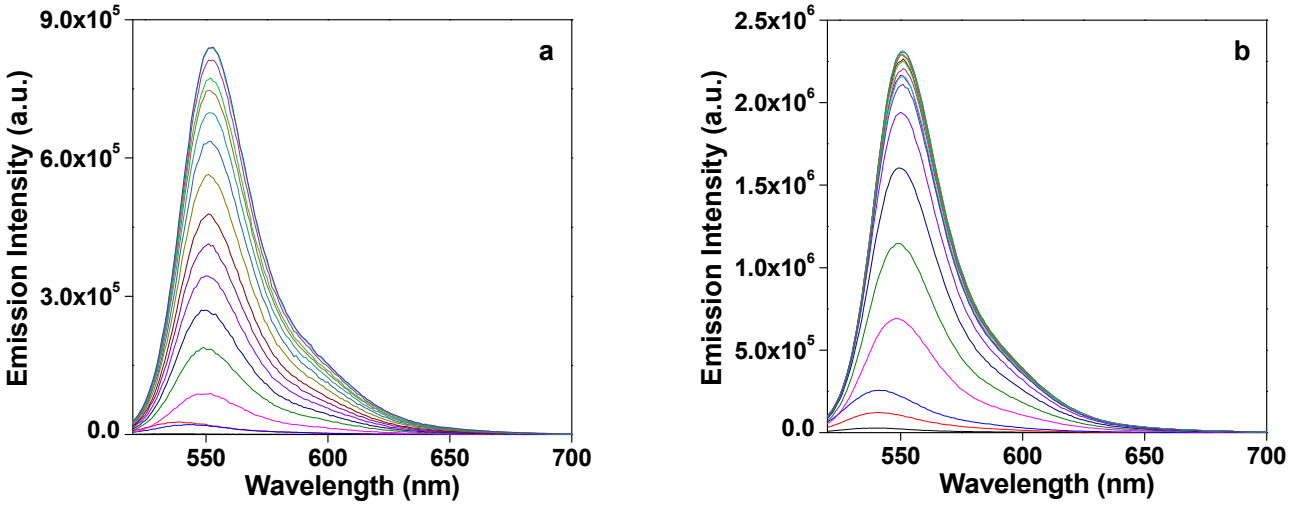

Fig. 9. Fluorescence spectra of **R6FMS** in the presence of different concentrations of (a) Al^{3+} (0-800 μM) and (b) Cu^{2+} (0-500 μM) in ethanol at 298 K.

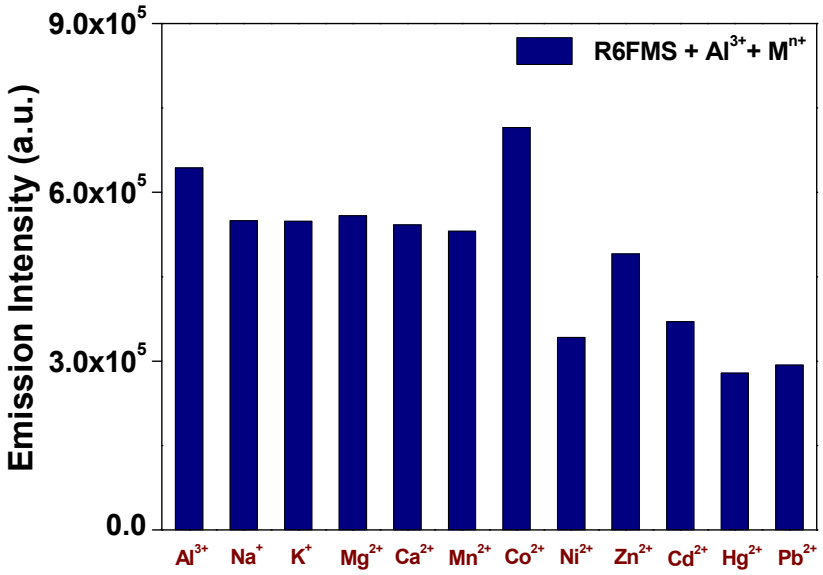

Fig. 10. Fluorescence intensity of **R6FMS** with Al^{3+} ions (800 μM) in the presence of two eqv. of other metal ions in ethanol at 298 K.

When fluorescence spectra of **R6FMS** have been analysed in the presence of different metal ions in water/acetonitrile (14:1, v/v) (pH 7.2, 10 mM HEPES buffer), its response towards Al^{3+}, Cr^{3+}, Fe^{3+}, Cu^{2+} and Hg^{2+} ions differs significantly from that in ethanol. Fluorescence intensity of the probe (0.033 g/L) increases at 546 nm appreciably in the presence of Cu^{2+} and Hg^{2+} ions upon excitation at 500 nm. It

is pertinent to mention that Al^{3+}, Cr^{3+} and Fe^{3+} ions, which caused significant emission enhancement of the probe in ethanol, are not able to increase its fluorescence intensity in water/acetonitrile (14:1, v/v) (pH 7.2, 10 mM HEPES buffer) (supplementary information, Fig. S9). Fluorescence intensity of the probe increases with the increase in concentration of Cu^{2+} and Hg^{2+}. The intensity reaches to saturation upon addition of 800 μM of the divalent cations. Fluorescence intensity increases by 36 and 14 times with Cu^{2+} and Hg^{2+} ions, respectively, in buffer solution (Fig. 11). Although fluorescence intensity of the probe with Cu^{2+} reduces when the medium is changed from ethanol to water, the enhancement in fluorescence intensity is still significantly high to detect this cation in water media. On the other hand, fluorescence enhancement of the probe with mercury ion increases when the solvent is changed from organic to aqueous media. That means Hg^{2+}, which cannot be identified with **R6FMS** in ethanol, now can be detected in aqueous medium with certainty with the same probe. Apart from that, all other relevant cations cannot induce any significant change in fluorescence properties of the probe in this medium, too. Fluorescence intensity of the probe with Hg^{2+} has been recorded in the presence of other cations to examine whether the process of detection of mercury ions is free of interference or not (Fig. 12). It has been found that there is no appreciable decrease in the fluorescence intensity of **R6FMS** with Hg^{2+} in the presence of Na^{+}, Al^{3+}, Cr^{3+}, Fe^{3+}, Mn^{2+}, Zn^{2+} and Pb^{2+} ions. So, the probe can be used to detect the cation in aqueous medium even in the presence of other cations.

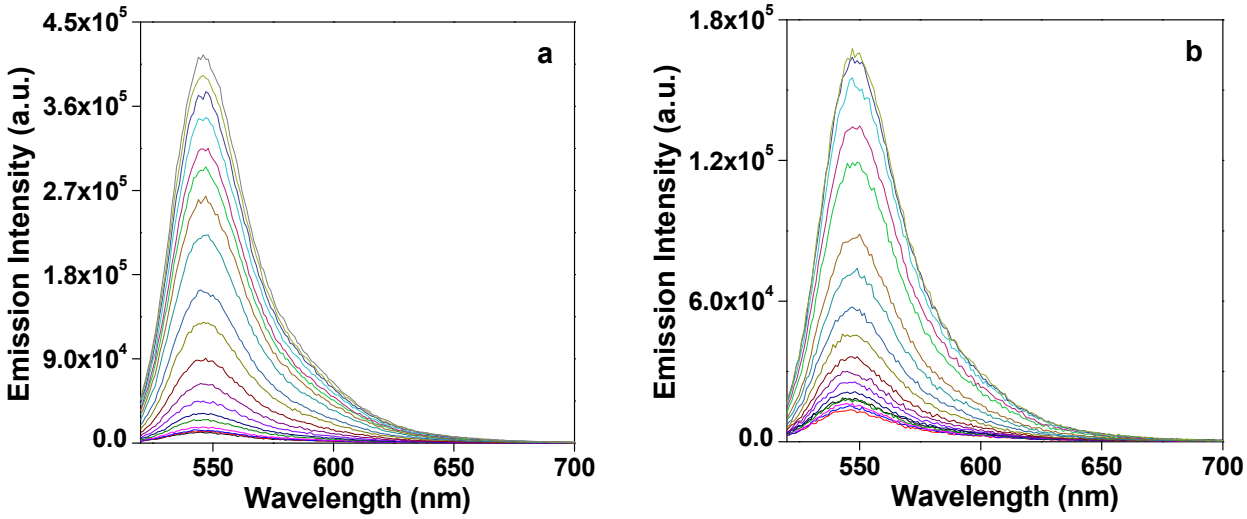

Fig. 11. Fluorescence spectra of **R6FMS** in the presence (0-800 μM) of (a) Cu^{2+} and (b) Hg^{2+} ions in 10 mM HEPES buffer in water/acetonitrile = 14:1 (v/v) (pH 7.2) at 298 K.

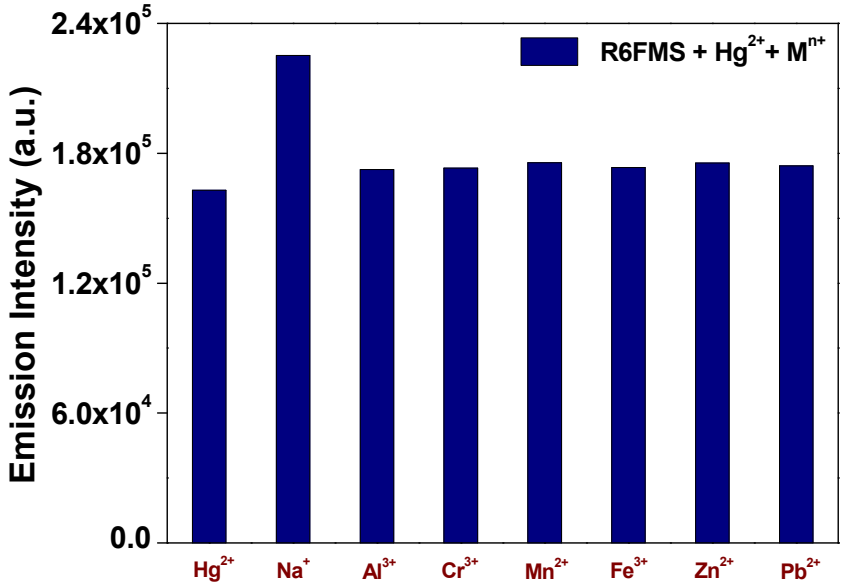

Fig. 12. Fluorescence intensity of **R6FMS** with Hg^{2+} (800 μM) in the presence of two eqv. of other metal ions in 10 mM HEPES buffer in water/acetonitrile = 14:1 (v/v) (pH 7.2) at 298 K.

Quantum yield is an important parameter to understand the changes in fluorescence properties. The quantum yield of the probe has been determined in ethanol as well as in water/acetonitrile (14:1, v/v) (pH 7.2, 10 mM HEPES buffer). The values are given in Table 3. In ethanol, quantum yield of the probe (**R6FMS**) is 0.057 while the value changes to 0.389, 0.275, 0.348 and 0.557 in the presence of Al^{3+}, Cr^{3+}, Fe^{3+} and Cu^{2+} ions, respectively. So, there is considerable enhancement in quantum yield of the probe upon its interaction with these cations. As the fluorescence enhancement of **R6FMS** has been observed only with Cu^{2+} and Hg^{2+} ions in water/acetonitrile (14:1, v/v) (pH 7.2, 10 mM HEPES buffer), quantum yield of the probe has been measured only with these ions in aqueous medium. The quantum yields have been determined to be 0.704 and 0.716 with Cu^{2+} and Hg^{2+} ions, respectively. Again, it could be mentioned that quantum yield of the probe enhances significantly with these divalent cations in aqueous medium.

Table 3. Quantum yield, lifetime and LOD values in ethanol and aqueous media at 298 K

Sl. No.	Species	Quantum yield	Life-time τ (ns)	LOD ($\times 10^{-7}$ M)
In ethanol				
1.	**R6FMS**	0.057	3.6233	---
2.	**R6FMS** + Al^{3+}	0.389	3.83	3.79
3.	**R6FMS** + Cr^{3+}	0.275	.3.66	14.80
4.	**R6FMS** + Fe^{3+}	0.348	3.73	3.27
5.	**R6FMS** + Cu^{2+}	0.557	4.16	0.74
In HEPES buffer (pH 7.2)				
6.	**R6FMS**	0.077	3.72	---
7.	**R6FMS** + Cu^{2+}	0.704	4.08	12.14
8.	**R6FMS** + Hg^{2+}	0.716	3.93	41.27

The lifetimes of **R6FMS** and **R6FMS** in the presence of the cations have been determined using time-correlated single photon counting (TCSPC) measurements (Table 3) in both ethanol (supplementary information, Fig. S10) and aqueous buffer (supplementary information, Fig. S11) media. In ethanol, life time values of **R6FMS** and Al^{3+}, Cr^{3+}, Fe^{3+} and Cu^{2+} bound materials are found to be 3.62, 3.83, 3.66, 3.73 and 4.16 ns, respectively. On the other hand, life times of **R6FMS** and Cu^{2+} and Hg^{2+}-bound **R6FMS** in aqueous buffer medium (pH 7.2) have been determined to be 3.72, 3.93 and 4.08 ns, respectively. If noticed closely at the figure, it reveals that decay profile of metal free material follows bi-exponential pathways while all the metal bound **R6FMS** materials show mono-exponential decay behavior. Thus, it is evident that life time of the silica material increases in the presence of all the cations in both the media.

Sensitivity of a probe is assessed by its limit of detection (LOD) values. Small LOD value refers to high sensitivity of the probe. LOD values of the probe towards Al^{3+}, Cr^{3+}, Fe^{3+}, Cu^{2+} and Hg^{2+} ions have been measured in appropriate medium following the 3σ method.[42] In ethanol, detection limits of **R6FMS** have been determined as 3.79 $\times 10^{-7}$ M, 1.48 $\times 10^{-6}$ M, 3.27 $\times 10^{-7}$ M and 7.4 $\times 10^{-8}$ M towards Al^{3+}, Cr^{3+}, Fe^{3+} and Cu^{2+}, respectively. Details are given in supplementary information, Fig. S12-S16. In water/acetonitrile (14:1, v/v) (pH 7.2, 10 mM HEPES buffer), LOD values have been measured to be 1.21 and 4.13 μM for Cu^{2+} and Hg^{2+} ions, respectively. Details on the determination of LOD in aqueous buffer medium are given in supplementary information, Fig. S17-S19. It is to note that sensitivity of the probe decreases towards Cu^{2+} when the solvent is changed from ethanol to buffer medium.

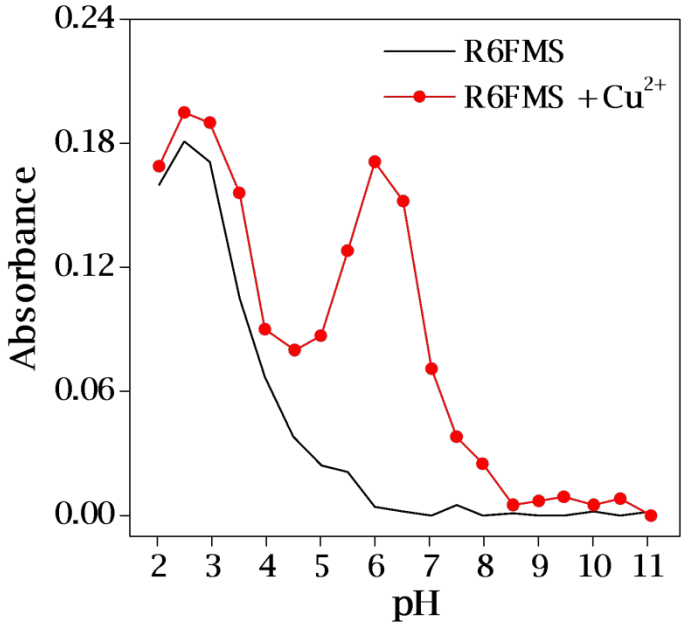

Fig. 13. Absorption intensity of **R6FMS** in absence and in the presence of Cu^{2+} at different pH at 298 K (*l* = 1 cm).

It has been checked whether the binding of **R6FMS** with the metal ions in both the media is reversible or not (supplementary information, Figure S20). For this purpose, reversible binding of the probe with Al^{3+} has been examined in ethanol using ammonium bifluoride (Fig. S20a). **R6FMS** shows high absorbance at 525 nm in the presence of Al^{3+}. Upon addition of F^- ion, absorbance decreases indicating that the anion snatches Al^{3+} from Al-probe complex. Again, when excess Al^{3+} is added, there is enhancement in absorbance. Thus, it is found that the binding of Al^{3+} with the probe is reversible in ethanol. On the other hand, binding of Hg^{2+} with the probe has been checked in aqueous buffer with Na_2-EDTA as well as Na_2S (Fig. S20b and c). Upon addition of Hg^{2+}, absorbance of the probe increases. However, on addition of Na_2-EDTA, absorbance of Hg-probe does not change. Addition of sulfide anion in place of Na_2-EDTA also gives similar results and the absorbance of the probe remains unchanged. Thus, both the results indicate that the binding of Hg^{2+} to **R6FMS** is not reversible in aqueous buffer.

pH change can affect absorption intensity of the probe in absence and in the presence of a cation which changes absorbance of the probe in aqueous medium (Fig. 13). Cu^{2+} has been chosen here for the study as an exemplary case. Absorption intensity of **R6FMS** is high at low pH region as under strong acidic condition as spirolactam ring of rhodamine derivative is opened under low pH region. As pH of the medium is changed from acidic to alkaline, the intensity of the free probe starts to decrease and flattens at around pH 6.0. However, the pattern is changed when Cu^{2+} is present in the system. The absorption intensity of the free probe is low under weakly acidic condition whereas its intensity is high with Cu^{2+}

under the same condition. Under weakly acidic condition or alkaline condition, spirolactam ring of the probe is closed and it becomes non-fluorescent. However, presence of Cu^{2+} causes opening of spirolactam ring of the probe under weakly acidic or alkaline condition and strong absorption intensity enhancement is observed. Further increase in pH of the medium actually decreases the fluorescence intensity as hydroxide of the metal ion may start precipitating out.

It is known that rhodamine derivatives are colorless and nonfluorescent when the spirocyclic ring is closed. When the ring opens, either due to metal binding or low pH, it shows pink color and strong fluorescence. From the above discussion it is evident that the mode of binding of trivalent Al^{3+} ion and bivalent Hg^{2+} ion, as representative cases, are different. Interaction of **R6FMS** with the two metal ions can be monitored by using different spectral techniques. NMR spectroscopy has been used in this study to understand the possible way of interaction of the metal ions with the rhodamine based chemosensor. ^{29}Si MAS NMR spectra and ^{13}C CP MAS NMR spectra of **R6FMS** have been recorded after its interaction with Al^{3+} and Hg^{2+} ions in the respective medium followed by filtration. The results lead to some significant conclusions. Before interaction with the cations, ^{29}Si MAS NMR spectrum of the probe exhibits peaks at −110.6, −102.3, −65.1 and −58.2 ppm (Fig. S21a). After interaction of the probe with aluminum ion in ethanol or mercury ion either in ethanol or HEPES buffer in water/acetonitrile, peaks are retained at similar positions (supplementary information, Fig. S21b-d, Table 2). This indicates that the silica framework remains unaffected due to interaction with the metal ions.

However, the ^{13}C CP MAS NMR spectra of the probe after its interaction with Al^{3+} and Hg^{2+} ions give some significant information on the nature of metal-probe interaction. The ^{13}C CP MAS NMR spectra of **R6FMS** after its interaction with Al^{3+} in ethanol, Hg^{2+} in ethanol and Hg^{2+} in HEPES buffer in water/acetonitrile are shown in Fig. 14. After the interaction with Al^{3+} ion, the ^{13}C CP MAS NMR spectrum of **R6FMS** shows only three peaks at 9.8, 21.4 and 43.3 ppm corresponding to the three carbon atoms of propyl group (Fig. 14b, Table 2). This is a drastic change in comparison to the spectrum of the probe alone shown in Fig. 14a. It indicates that the probe does not retain its original structure on binding with Al^{3+} and cleaves into two parts as proposed in Scheme 2. Probably, Al^{3+} catalyzes the hydrolysis of imine bond and detaches the bisphenol A bound rhodamine unit from the silica framework while the 3-APTES moiety remains attached to **MS**. When Al^{3+} is added to **R6FMS** in ethanol a pink coloration is observed, with increment in absorbance at 525 nm and strong fluorescence at 552 nm, indicating opening of spirocyclic ring of the probe. Al^{3+} induces the spirolactam ring opening followed by coordination with the ring opened probe and the color, absorbance and fluorescence originates from the Al^{3+}-bound complex which remains in the solution of ethanol along with the detached 3-APTES bound solid silica. This has been further supported by filtration of this ethanolic mixture to separate the silica matrix from the Al^{3+}-bound rhodamine derivative (supplementary information, Figure S22A). It is found that the color of the

Al^{3+}-bound rhodamine is transferred completely in the filtrate. This has also been supported by the absorption spectra of the solution before and after filtration (Fig. S22B). The absorption spectra show the band at 525 nm indicating existence of the same ring opened species in the solutions before and after filtration. The solid silica residue does not retain pink color of the complex and its color also changes from the original probe, **R6FMS**. This explains the reason behind observing only three peaks in the ^{13}C CP MAS NMR spectrum of the solid silica framework bound to 3-APTES obtained after filtration.

On the other hand, the ^{13}C CP MAS NMR spectrum of **R6FMS** after its interaction with Hg^{2+} in ethanol (Fig. 14c) shows peaks which are not similar to either free **R6FMS** or **R6FMS** after its interaction with Al^{3+}. The nature of the interaction of **R6FMS** with Hg^{2+} under this condition is inconclusive. Since **R6FMS** is unable to detect Hg^{2+} in ethanol, further studies have not been carried out with this material. The ^{13}C CP MAS NMR spectrum of **R6FMS** after its interaction with Hg^{2+} in HEPES buffer solution (Fig. 14d) again shows distinctly different signals than that of Al^{3+} or Hg^{2+}-interacted **R6FMS** in ethanol (Fig. 14b and c). Peaks of ^{13}C CP MAS NMR spectrum of **R6FMS** after its interaction with Hg^{2+} are given in Table 2. Many of these peaks could also be found in the spectrum of the probe, **R6FMS**. It is to be noted that the peak at 66.3 ppm which is present in **R6FMS** disappears on binding with Hg^{2+} in aqueous media. This indicates the opening of the spirocyclic ring of rhodamine unit anchored to the silica support by the cation.[43, 44] As ^{29}Si MAS NMR spectrum of Hg^{2+}-bound probe in buffer medium (Fig. S20d) confirms retention of silica framework and ^{13}C CP MAS NMR spectrum (Fig. 14d) shows appearance of all the peaks corresponding to bisphenol A and rhodamine framework, it may be concluded that Hg^{2+} has been able to induce opening of the spirocyclic ring without catalyzing the cleavage of the imine bond (Scheme 2). Thus, in buffer medium Hg^{2+} induces opening of spirolactam ring followed by the coordination of Hg^{2+} center with the ring opened probe keeping the fluorophoric unit attached to the silica support.

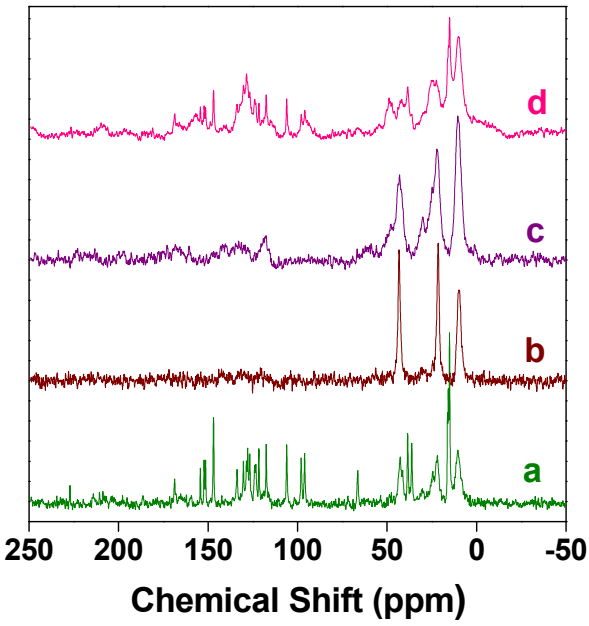

Fig. 14. Solid state ^{13}C CP-MAS NMR spectra of(a) **R6FMS**, (b) Al^{3+}-**R6FMS** in ethanol medium, (c) Hg^{2+}-**R6FMS** in ethanol medium and (d) Hg^{2+}-**R6FMS** in HEPES buffer in water/acetonitrile.

It has been revealed that **R6FMS** is able to sense Al^{3+}, Cr^{3+}, Fe^{3+} and Cu^{2+} ions in ethanol while Cu^{2+} and Hg^{2+} ions in water/acetonitrile (14:1, v/v) (pH 7.2, 10 mM HEPES buffer). The different behavior of the probe in these solvents may be ascribed to different binding affinity of the solvent and/or rhodamine functionalized material towards different metal ions.[45] Trivalent cations such as Al^{3+} ions have very strong affinity towards water and are unable to open the spirolactam ring in aqueous medium possibly due to their strong coordination with water molecules. On the other hand, Cu^{2+} is able to open the spirocyclic in both the media.

Removal of Cu^{2+} and Hg^{2+} ions from aqueous solution

As fluorescence intensity of **R6FMS** changes significantly with Cu^{2+} and Hg^{2+} ions in aqueous media indicating its ability to sense the cations by opening the spirocyclic followed by coordination, the probe has been used to remove these cations from aqueous medium. The study has been accomplished using atomic absorption spectroscopy (AAS). Concentration of metal ion in the solutions has been determined before and after treatment with **R6FMS**. Metal ion removal capacity (Q) of **R6FMS** has been determined with the following formula:[46]

$$Q = (C_i - C_f)/C_f \times 100\%$$

where C_i and C_f are the concentration of the metal cation before and after the treatment with **R6FMS**.

When Cu^{2+} ion solution of initial concentration 50 ppm has been treated with 0.025 g of **R6FMS**, the final concentration in the filtrate is found to be 14.5 ppm. When 0.025 g of **R6FMS** has been treated with an 88 ppm Hg^{2+} ion solution, the final concentration of Hg^{2+} in the filtrate is found to be 21.6 ppm. Therefore, removal efficiency of the material has been calculated to 71 and 75.4% for Cu^{2+} and Hg^{2+}, respectively. These facts indicate that the functionalized mesoporous silica-based probe is effective to remove the metal ions. **R6FMS** has been treated with excess amount of Cu^{2+} and Hg^{2+} ions to calculate maximum adsorption capacity of the silica material. The maximum adsorption capacity of **R6FMS** is found to be 35 mg/g and 148 mg/g for Cu^{2+} and Hg^{2+}, respectively. These results are well in agreement with the SEM-EDS analyses (supplementary information, Fig. S23-S26) carried out with the metal-exchanged solid samples of **R6FMS**.

Comparative discussion

Several parameters of recently published materials along with the present work are given in Table 4 to compare the different aspects. Different types of probes are included in this table where the materials have been used for identification or separation of a species or both.[34, 44, 47-55] A number of metal ions could be detected and removed, if any, with the help these compounds. Many of the probes are used for colorimetric detection only (Table 4, entry 3-8). The present study reports colorimetric as well as fluorometric sensing of multiple cations. Generally, fluorometric methods show better sensitivity. In the present study, excitation wavelength is 500 nm (also for Table 4, entry 10-12). Probes with higher excitation and emission wavelength, as in the present case, are desirable because they could be used in biological domain as low wavelength excitation may kill living cells. Although many probes show better sensitivity towards Al^{3+}, Cr^{3+} and Fe^{3+} ions (for example, Table 4, entry 11 and 12), LOD values of **R6FMS** indicates very good sensitivity towards these cations. Many of the materials including **R6FMS** can perform sensing as well as separation of the cationic species (Table 4, entry 1-6, 11). However, a few of them can either separate the metal ions (Table 4, entry 7 and 8) or sense them (Table 4, entry 9, 10 and 12). Most of the listed materials including **R6FMS** have been used in various applications. Maximum adsorption capacity of the probes for Cu^{2+} has been similar (Table 4, entry 2, 7, 8 and 14). For separation of Hg^{2+}, maximum adsorption capacity of **R6FMS** displays better value than the probe in Table 4, entry 4. The most striking factor of the present study is that the probe can detect a number of metal ions and the sensing of these cations is dependent on solvent. If the solvent is changed, the probe can sense a particular set of cations.

Table 4. A few aspects of some recently published related materials

Entry	Probe	Metal ion(s)	Excitation/ Emission wavelength (nm)	LOD	Sensing and removal?	Solvent effect	Applications	Maximum adsorption capacity	Ref.
1	A tryptophan-dithiocarbamate-based fluorescent polymeric probe	Hg^{2+}	285/366	1.5 nM (300 ppt)	Yes	No	Cell imaging	---	47
2	Quaternized salicylaldehyde Schiff base modified SBA-15 mesoporous silica	Cu^{2+} (Turn off)	369/490	3.7×10^{-7} M	Yes	No	Removal	34.73 mg/g	48
3	Chitosan–gold nanocomposite	Hg^{2+} (Colorimetric)	---	3.2×10^{-9} M	Yes	No	'Real' sample analysis	---	49
4	SBA-16 doped with a cationic porphyrin bearing imidazolium substituents	Cu^{2+}, Pb^{2+} and Hg^{2+} (Colorimetric)	---	5.8 ppm (Pb^{2+}), 3.8 ppm (Hg^{2+}) and 3.6 ppm (Cu^{2+})	Yes	No	Removal of Hg^{2+}	69 mg/g (Hg)	50
5	Silica Nanospheres-Coated Nanofibrillated Cellulose	Cu^{2+} (Colorimetric)	---	1.2×10^{-6} M	Yes	No	---	2.62 mmol/g	51
6	Glycylglycine-Based	Cu^{2+}	---	317	Yes	No	---	For the	52

	Polymer	(Colorimetric)		parts per billion (5 μM)				complete removal of 1.0 mg (0.015 mmol) cation, 55 mg (0.034 mmol) of polymer needed	
7	N-propyl-2-pyridylimine functionalized SBA-15	Cu^{2+} and Pb^{2+}	---	---	Only removal	---	---	35.87 mg/g (Cu) 82.05 mg/g (Pb)	53
8	Ethylenediaminepropyl-2-pyridylimine functionalized SBA-15	Cu^{2+} and Pb^{2+}	---	---	Only removal	---	---	48.26 mg/g (Cu) 106.62 mg/g (Pb)	
9	SBA-15 functionalized with 5-(4-carboxy-phenylazo)-8-hydroxyquinoline	Pb^{2+}	350/429	4.90×10^{-7} M	Only sensing	No	Water analysis	---	54
10	Rhodamine 6G on mesoporous silica	Fe^{3+}	510/552	---	Only sensing	No	Cell imaging and microfluidic chips	----	55

11	Rhodamine functionalized mesoporous silica (**RFMS**)	Al^{3+}, Cr^{3+} and Fe^{3+}	500/550	5.40 nM (Al), 9.18 nM (Cr) and 722.80 nM (Fe)	Yes	No	Removal of these cations	11.20 mg/g (Al), 19.72 mg/g (Cr) and 21.55 mg/g (Fe)	34
12	Bromosalicylaldehyde incorporated rhodamine 6G	Al^{3+}, Cr^{3+} and Fe^{3+}	500/552	1.18 nM (Al), 1.80 nM (Cr) and 4.04 nM (Fe)	Only sensing	No	Logic gates	---	44
13	Rhodamine and bisphenol A functionalized mesoporous silica (**R6FMS**)	Al^{3+}, Cr^{3+}, Fe^{3+} Cu^{2+} (in ethanol)	500/550	3.79×10^{-7} M (Al), 1.48 μM (Cr), 3.27×10^{-7} M (Fe) and 7.4×10^{-8} M (Cu)	Only sensing	Yes	---	---	Present work
14	Rhodamine and bisphenol A functionalized mesoporous silica (**R6FMS**)	Cu^{2+} and Hg^{2+} (in water)	500/546	1.21 μM (Cu) and 4.13 μM (Hg)	Yes	Yes	Removal of these cations	35 mg/g and 148 mg/g for Cu^{2+} and Hg^{2+},	

Conclusions

We have synthesized a rhodamine anchored mesoporous silica material (**R6FMS**) through incorporation of bisphenol A moiety. It has been characterized by several standard techniques. **R6FMS** has been able to detect several cations such as Al^{3+}, Cr^{3+}, Fe^{3+} and Cu^{2+} in pure ethanol while in HEPES buffer, the probe could sense Cu^{2+} and Hg^{2+} by changing its color as well as increasing fluorescence intensity at ~550 nm. There are significant increments in quantum yield of the silica material upon interaction with the cations. Life time of the probe also increases on interaction with the cations. Rhodamine derivatives are colorless and nonfluorescent when they are in closed spirocyclic form. However, they are pink and strongly fluorescent when the ring is opened. These cations have been able to open the spirolactam ring to show changes in color and fluorescence. However, detailed studies indicate that Hg^{2+} in buffer is able to open the spirolactam ring in buffer whereas Al^{3+} induces opening of spirocyclic ring in ethanol as well as catalyses hydrolysis of imine bond. Such hydrolysis leads to the cleavage of imine bond and the rhodamine part along with bisphenol A counterpart leaves the silica framework. Thus, Al^{3+}-bound rhodamine species comes in the solution phase making the separation process using silica framework impossible by simple filtration. In case of Hg^{2+}, there is no hydrolysis of imine bond of the probe but only opening of spirolactam ring of rhodamine unit followed by coordination with Hg^{2+}-center in water. This motivated us to remove the Cu^{2+} and Hg^{2+} ions from aqueous solution using **R6FMS**. It shows moderate efficiency for the removal of these cations from water. Thus, we can conclude that **R6FMS** is able to sense Al^{3+}, Cr^{3+}, Fe^{3+} and Cu^{2+} in ethanol while it discriminates divalent cations, Cu^{2+} and Hg^{2+}, from these trivalent cations by sensing and removing them from aqueous medium.

Conflicts of interest

There are no conflicts to declare.

Acknowledgements

MN gratefully acknowledges financial support from WB-DST, India (ST/P/S&T/15G-20/2018). AP wishes to thank UGC, New Delhi for providing her a fellowship. HU thankfully acknowledges financial support from JST-Mirai Program (JPMJMI18E3) and JSPS KAKENHI Grants (20H02797). PR wishes to thank CSIR, New Delhi (Sanction letter no. 01 (2993)/19/EMR-II). Authors are thankful to N Pradhan of Indian Association for the Cultivation of Science, Kolkata for providing TEM facilities, G Ghosh of Visva-Bharati for AAS studies and DST-PURSE Project, Visva-Bharati, for FE-SEM facilities.

References

1. S. Das, M. Dutta and D. Das, *Anal. Methods*, 2013, **5**, 6262-6285.
2. A. Gupta and N. Kumar, *RSC Adv.*, 2016, **6**, 106413-106434.
3. P. Roy, *Dalton Trans*., 2021, **50**, 7156-7165.
4. A. Roy, M. Nandi and P. Roy, *Trends Anal. Chem.*, 2021, **138**, 116204.
5. P. Roy, *Coord. Chem. Rev.*, 2021, **427**, 213562.
6. A. Roy, U. Shee, A. Mukherjee, S. K. Mandal and P. Roy, *ACS Omega*, 2019, **4**, 6864−6875.
7. Z. Li, J. Wang, L. Xiao, J. Wang and H. Yan, *Inorg. Chim. Acta*, 2021, **516**, 120147.
8. D. Maity and T. Govindaraju, *Chem. Commun.*, 2012, **48**, 1039-1041.
9. J. Wang, W. Lin and W. Li, *Chem. Eur J.*, 2012, **18**, 13629-13632.
10. N. Ahfad, G. Mohammadnezhad, S. Meghdadi and H. Farrokhpour, *Spectrochim. Acta Part A*, 2020, **228**, 117753.
11. W. Cao, X.-J. Zheng, J.-P. Sun, W.-T. Wong, D.-C. Fang, J.-X. Zhang and L.-P. Jin, *Inorg. Chem.*, 2014, **53**, 3012–3021.
12. M. Yu, R. Yuan, C. Shi, W. Zhou, L. Wei and Z. Li, *Dyes Pigm.*, 2013, **99**, 887–894.
13. J. Sun, T.-r. Li, C. Liu, J. Xue, L.-m. Tian, K. Liu, S.-l. Li and Z.-y. Yang. *J. Photochem. Photobiol. A*, 2021, **406**, 113007.
14. K. Tsukamoto, Y. Shinohara, S. Iwasaki and H. Maeda, *Chem. Commun.*, 2011, **47**, 5073-5075.
15. D. Das, R. Alam, A. Katarkar and M. Ali, *Photochem. Photobiol. Sci.*, 2019, **18**, 242-252.
16. A. Roy, S. Das, S. Sacher, S. K. Mandal and P. Roy, *Dalton Trans.*, 2019, **48**, 17594–17604.
17. S. Paul, A. Manna and S. Goswami, *Dalton Trans.*, 2015, **44**, 11805–11810.
18. M. Wang, F. Yan, Y. Zou, L. Chen, N. Yang and X. Zhou, *Sens. Actuators B*, 2014, **192**, 512–521.
19. Y. Yang, C. Gao, B. Li, L. Xu and L. Duan, *Sens. Actuators B*, 2014, **199**, 121–126.
20. M. Ozdemir, *J. Photochem. Photobiol. A*, 2016, **318**, 7–13.
21. A. K. Das, Bioinorganic Chemistry, Books & Allied, Kolkata, 2007.
22. C. C. Willhite, N. A. Karyakina, R. A. Yokel, N. Yenugadhati, T. M. Wisniewski, I. M. F. Arnold, F. Momoli and D. Krewski, *Crit. Rev. Toxicol.*, 2014, **44**, 1–80.
23. C. Liu and X. Luo, *J. Mater. Chem. B*, 2021, **9**, 2736-2746.
24. Y. Liu, M. Nguyen, A. Robert and B. Meunier, *Acc. Chem. Res*., 2019, **52**, 2026−2035.
25. D. G. Munoz, *Arch. Neurol*., 1998, **55**, 737−739.
26. T. W. Clarkson and L. Magos, *Crit. Rev. Toxicol.*, 2006, **36**, 609–662.
27. D. O'Connor, D.Y. Hou, Y.S. Ok, J. Mulder, L. Duan, Q. R. Wu, S. X. Wang, F.M.G. Tack and J. Rinklebe, *Environ. Int.*, 2019, **126**, 747–761.
28. J. Wu, F. Xu, S. Li, P. Ma, X. Zhang, Q. Liu, R. Fu and D. Wu, *Adv. Mater.*, 2019, **31**,

1802922.

29. S. Halder, J. Mondal, J. Ortega-Castro, A. Frontera and P. Roy, *Dalton Trans.*, 2017, **46**, 1943–1950.
30. S. Ramanayaka, M. Vithanage, A. Sarmah, T. An, K.-H. Kim and Y. Sik Ok, *RSC Adv.*, 2019, **9**, 34359–34376.
31. K. Li, J.-j. Li, N. Zhao, T.-t. Xie, B. Di and L.-l. Xu, *Dalton Trans.*, 2019, **48**, 17800–17809.
32. T. Das, A. Roy, H. Uyama, P. Roy and M. Nandi, *Dalton Trans.*, 2017, **46**, 7317–7326.
33. T. Das, D. Singha, A. Pal and M. Nandi, *Sci. Rep.*, 2019, **9**, 19378.
34. D. Singha, T. Das, L. Satyanarayana, P. Roy and M. Nandi, *New J. Chem.*, 2019, **43**, 15563–15574.
35. D.D. Perrin, W.L.F. Armarego and D.R. Perrin, Pergamon Press, Oxford, UK, 1980.
36. S. Erdemir, O. Kocyigit and S. Malkondu, *J. Fluoresc.*, 2015, **25**, 719–727.
37. L. Bing, *Sens. Actuator B*, 2014, **198**, 342–349.
38. A. M. Brouwer, Pure Appl. Chem., 2011, **83**, 2213–2228.
39. S. Inagaki, Y. Fukushima and K. Kuroda, J. Chem. Soc., *Chem. Commun.*, 1993, 680–682.
40. A. Grosman and C. Ortega, *Langmuir*, 2005, **21**, 10515–10521.
41. S. Inagaki, S. Guan, Y. Fukushima, T. Ohsuna and O. Terasaki, *J. Am. Chem. Soc*., 1999, **121**, 9611–9614.
42. V. Thomsen, D. Schatzlein and D. Mercuro, *Spectroscopy*, 2003, **18**, 112–114
43. B. Sen, M. Mukherjee, S. Banerjee, S. Pal and P. Chattopadhyay, *Dalton Trans.*, 2015, **44**, 8708–8717.
44. S. Dey, S. Sarkar, D. Maity and P. Roy, *Sens. Actuators B*, 2017, **246**, 518–534.
45. M. Yu, R. Yuan, C. Shi, W. Zhou, L. Wei and Z. Li, *Dyes Pigm.*, 2013, **99**, 887–894.
46. F. Luo, J. L. Chen, L. L. Dang, W. N. Zhou, H. L. Lin, J. Q. Li, S. J. Liu and M. B. Luo, *J. Mater. Chem. A*, 2015, **3**, 9616–9620.
47. N. Choudhury, B. Saha, B. Ruidas and P. De, *ACS Appl. Polym. Mater*., 2019, **1**, 461−471.
48. Y. Zhang, X. Cao, G. Wu, J. Wang and T. Zhang, *Appl. Surf. Sci*., 2020, **527**, 146803.
49. L. Hu, B. Zhu, L. Zhang, H. Yuan, Q. Zhao and Z. Yan, *Analyst*, 2019, **144**, 474–480.
50. G. A. Marcelo, S. M.G. Pires, M. A. F. Faustino, M. M.Q. Simões, M. G. P.M.S. Neves, H. M. Santos, J. L. Capelo, J. P. Mota, C. Lodeiro and E. Oliveir, *Dyes Pigm*., 2019, **161**, 427–437.
51. A. M. Yousif, O. F. Zaid, W. A. El-Said, E. A. Elshehy and I. A. Ibrahim, *Ind. Eng. Chem. Res*., 2019, **58**, 4828−4837.
52. N. Choudhury, S. Mete, S. Kambalapalli and P. De, *J. Polym. Sci., Part A*, 2018, **56**, 914–921.
53. Y. Zhang, X. Cao, J. Sun, G. Wu, J. Wang and D. Zhang, *J. Sol-Gel Sci. Technol*., 2019, **94**, 658-

670.

54. L. Zhao, D. Suib and Y. Wang, *RSC Adv.*, 2015, 5, 16611–16617.

55. H. Kim, B.A. Rao, J. Jeong, S. Angupillai, J.S. Choi, J.-O. Nam, C.-S. Lee and Y.-A. Son, *Sens. Actuators B*, 2016, **224**, 404-412.